Photodissociation Dynamics of the Chromophores of the Amino Acid Tyrosine: *p*-Methylphenol, *p*-Ethylphenol, and *p*-(2-Aminoethyl)phenol†

Chien-Ming Tseng,[‡,§] Yuan T. Lee,[‡,§] Chi-Kung Ni,*[,‡,||] and Jia-Lin Chang*[,⊥]

Institute of Atomic and Molecular Sciences, Academia Sinica, P.O. Box 23-166, Taipei, 10617 Taiwan, Department of Chemistry, National Taiwan University, Taipei, Taiwan, Department of Chemistry, National Tsing Hua University, Hsinchu, Taiwan, and Department of Science Application and Dissemination, National Taichung University, Taichung 403, Taiwan

Received: December 27, 2006; In Final Form: March 7, 2007

The photodissociation of *p*-methylphenol, *p*-ethylphenol, and *p*-(2-aminoethyl)phenol, chromophores of the amino acid tyrosine, was studied separately for each compound in a molecular beam at 248 nm using multimass ion imaging techniques. They show interesting side-chain size-dependent dissociation properties. Only one dissociation channel, that is, H atom elimination, was observed for both *p*-methylphenol and *p*-ethylphenol. The photofragment translational energy distributions and potential energy surfaces from ab initio calculation suggest that H atom elimination occurs from a repulsive excited state. On the other hand, the H atom elimination channel is quenched completely by internal conversion and/or intersystem crossing in *p*-(2-aminoethyl)phenol. Only C−C bond cleavage was observed from *p*-(2-aminoethyl)phenol. The photofragment translational energy distribution shows a slow component and a fast component. The fast component results from dissociation on an electronic excited state, but the slow component occurs only after the internal conversion to the ground electronic state. Comparison with the photodissociation of phenol and ethylbenzene is made.

I. Introduction

The amino acids are some of the most important biomolecules. Aromatic amino acids like tyrosine, tryptophan, and phenylalanine have very large UV absorption cross sections. However, the fluorescence quantum yields of these molecules are very small. They indicate the existence of fast nonradiative processes, which efficiently quench the fluorescence.[1−4] The nonradiative process was assumed to be the ultrafast internal conversion.[2−5] As soon as the electronic energy becomes vibrational energy after internal conversion, the highly vibrationally excited molecules quickly dissipate the vibrational energy to the surrounding molecules through intermolecular energy transfer before chemical reactions take place. This so-called photostability prevents the unnecessary photochemical reactions of these molecules upon UV irradiation.

Phenol is a chromophore of the amino acid tyrosine. Recent ab initio calculation suggests that the low fluorescence quantum yield of phenol is due to the dissociative character of the electronic excited-state potential energy surface, instead of fast internal conversion to the electronic ground state.[6−8] The calculation shows that absorption of UV photons in the range 290−240 nm corresponds to the photoexcitation of phenol to the S_1 $\pi\pi^*$ excited state. The second excited state has a significant antibonding σ^* character with respect to the OH bond distance. The population of the bright state, S_1, can be transferred to the dark state, S_2, through a conical intersection. As a result, instead of internal conversion to the ground electronic state, predissociation through $\pi\pi^*$ and $\pi\sigma^*$ coupling results in rapid quenching of the fluorescence. Indeed, the H atom elimination from the repulsive electronic excited state of phenol has been verified in a recent molecular beam experiment.[9] A similar dissociation channel was also observed from indole, a chromophore of the amino acid tryptophan.[10]

Since phenol is different from tyrosine—it lacks a side chain of the functional group $CH_2CH(NH_2)COOH$, it would be very interesting to determine the photodissociation properties when the chemical functional group is added to phenol. In this work, we reported the photodissociation of *p*-methylphenol, *p*-ethylphenol, and *p*-(2-aminoethyl)phenol. We demonstrate that the dissociation properties could change dramatically as the side chain is added to phenol.

II. Experimental

The multimass ion imaging techniques have been described in detail in our previous reports,[11−14] and only a brief account is given here. *p*-Methylphenol (or *p*-ethylphenol) vapor was formed by flowing ultrapure Ne at a pressure of 600 Torr through a reservoir filled with a *p*-methylphenol (or *p*-ethylphenol) sample at 80 °C. The *p*-methylphenol (or *p*-ethylphenol)/Ne mixture was transferred through a 90 °C flexible stainless steel tube to a pulsed valve and then expanded through a 500 μm high-temperature (100 °C) nozzle to form the molecular beam. The method to generate a *p*-(2-aminoethyl)phenol molecular beam is different from that of *p*-methylphenol. A glass container which contains a *p*-(2-aminoethyl)phenol solid sample located inside a stainless steel oven (100 °C) was attached to the front of a pulsed valve. The plunger of the pulsed valve extended to the exit hole (diameter: 500 μm) of the oven. The molecular beam was formed by expanding the *p*-(2-aminoethyl)-phenol/Ne mixture at a pressure of 600 Torr through the exit hole of the oven.

† Part of the special issue "M. C. Lin Festschrift".

* Corresponding authors. E-mail: ckni@po.iams.sinica.edu.tw (Ni); jlchang@mail.ntcu.edu.tw (Chang).

‡ Academia Sinica.

§ National Taiwan University.

|| National Tsing Hua University.

⊥ National Taichung University.

10.1021/jp068968q CCC: $37.00
Published on Web 04/21/2007

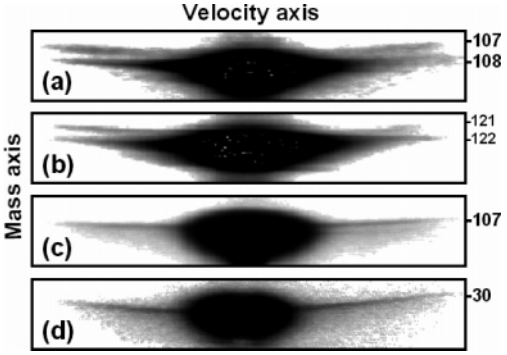

Figure 1. Photofragment ion images from (a) methylphenol, (b) ethylphenol, (c) and (d) *p*-(2-aminoethyl)phenol.

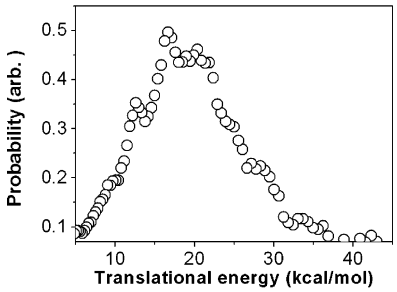

Figure 2. Photofragment translational energy distribution of the reaction $CH_3C_6H_4OH \rightarrow CH_3C_6H_4O + H$.

Molecules in the molecular beam were photodissociated by UV laser pulses, and fragments were then ionized by VUV laser pulses. The distance and time delay between the VUV laser pulse and the photolysis laser pulse were set such that the VUV laser beam passed through the center-of-mass of the dissociation products and generated a line segment of photofragment ions through the center-of-mass of the dissociation products by photoionization. To separate the different masses within the ion segment, a pulsed electric field was used to extract the ions into a mass spectrometer after ionization. At the exit port of the mass spectrometer, a two-dimensional ion detector was used to detect the ion positions and intensity distribution. In this two-dimensional detector, one direction was the recoil velocity axis and the other was the mass axis.

III. Computational

The geometries of the ground states and some low-lying conformers of *p*-methylphenol, *p*-ethylphenol, and *p*-(2-aminoethyl)phenol were optimized at the B3LYP/6-311++G(d, p) level. Harmonic vibrational frequencies were calculated to confirm that the obtained geometries correspond to the equilibrium structures. In order to interpret the experimental observations, we computed the potential energy curves for the ground and excited states of these molecules as functions of the O−H distance, in intervals of 12 pm, while fixing the other geometrical parameters at their equilibrium values. The potential energy curves were calculated by using the state-averaged complete active space self-consistent field (CASSCF) method with the 6-311++G(d, p) basis set. The active space adopted in the CASSCF calculations was ten electrons distributed in ten orbitals, denoted as (10, 10). All the calculations were performed using the MOLPRO 2006.1 package.[15]

IV. Results

***p*-Methylphenol.** The only fragment ion we observe from the photodissociation of *p*-methylphenol at 248 nm using the 118 nm photoionization laser beam is $m/e = 107$, corresponding to the heavy fragment from the H atom elimination channel. The photofragment ion images are shown in Figure 1a, and the corresponding translational energy distribution is shown in Figure 2. The probability distribution in the region less than 5 kcal/mol is obscured by the strong interference from parent molecules. Only the distribution larger than 5 kcal/mol is illustrated. It shows that the average released translational energy is large, and the peak of the distribution is located at 18 kcal/mol. It is interesting to note that the maximum translational energy almost reaches the maximum available energy of the reaction. These are the characteristics of the dissociation from an excited state of a repulsive potential or from an electronic state with a large exit barrier height.

The translational energy distribution is very similar to that of H atom elimination from photodissociation of phenol at 248 nm. The large translational energy release in the H atom elimination channel of phenol at 248 nm was explained as the dissociation from a repulsive potential energy surface.[9] Indeed, a similar repulsive potential energy surface along the O−H bond distance of *p*-methylphenol was also found from our calculation. Figure 3 shows potential energy curves of the first four singlet

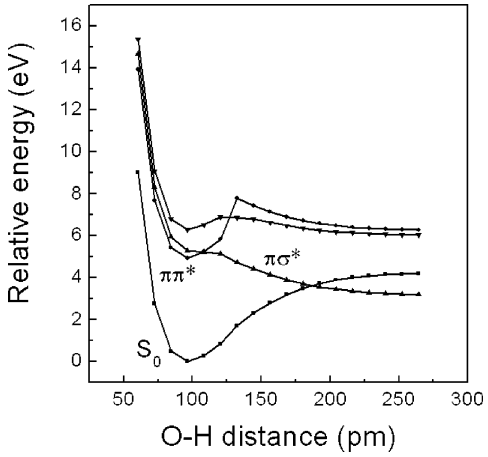

Figure 3. Potential energy curves of *p*-methylphenol as functions of the O−H distance calculated at the CASSCF(10,10)/6-311++G(d, p) level.

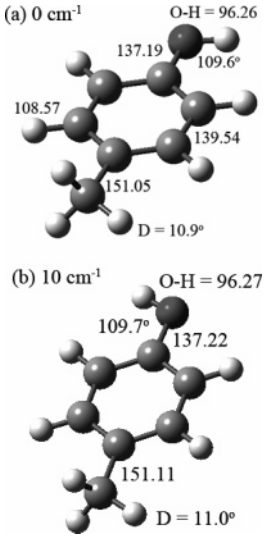

Figure 4. B3LYP/6-311G++(d, p) optimized equilibrium structures of the ground-state *p*-methylphenol and relative energies of two conformers with selected bond lengths (in pm) and bending angles. D is the dihedral angle between the methyl group and the benzene ring (nearly parallel).

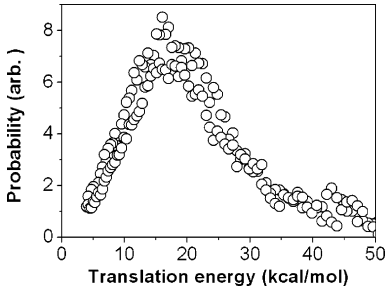

Figure 5. Photofragment translational energy distribution of the reaction $C_2H_5C_6H_4OH \rightarrow C_2H_5C_6H_4O + H$.

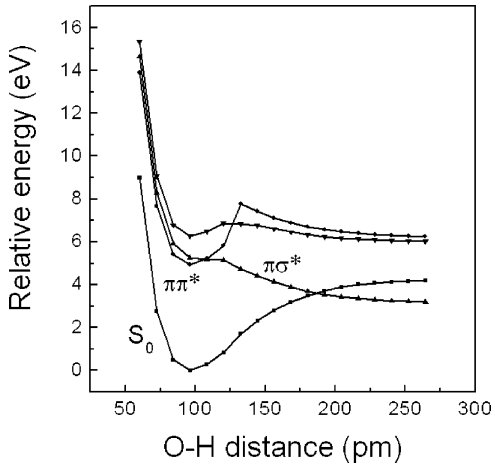

Figure 6. Potential energy curves of *p*-ethylphenol as functions of the O−H distance calculated at the CASSCF(10,10)/6-311++G(d, p) level.

electronic states along the O−H bond distance. The ground state is a stable state with respect to the O−H bond distance. The first electronic excited state, $\pi\pi^*$, shows a potential well at a short O−H bond distance. It crosses with a repulsive potential, $\pi\sigma^*$, at a large O−H bond distance. This calculation suggests that methylphenol can dissociate through the repulsive potential energy surface as long as the excitation energy is large enough to overcome the barrier height at the crossing point.

The fragment translational energy distribution and potential energy surfaces suggest that the H atom elimination occurs from the repulsive potential surface along the O−H bond (eq 1):

$$CH_3C_6H_4OH \rightarrow CH_3C_6H_4O + H \qquad (1)$$

The potential energy curves in Figure 3 were calculated at the ground-state geometry of the most stable conformer. The structure is shown in Figure 4a. The ground-state structure of the other stable conformer is shown in Figure 4b. For this conformer, we calculated the three lowest-lying states at two structures, one at the equilibrium structure of the ground state and the other at O−H = 210 pm. It was found that while the $\pi\sigma^*$ state lies higher than the ground state and the $\pi\pi^*$ state at the structure of the ground state, it becomes the lowest one at O−H = 210 pm. Accordingly, the potential energy curve of the $\pi\sigma^*$ state must intersect somewhere with that of the $\pi\pi^*$ state and that of the ground state, respectively, similar to those in Figure 3.

***p*-Ethylphenol.** Similar dissociation dynamics was found from the photodissociation of *p*-ethylphenol at 248 nm. Only the fragment ion of $m/e = 121$ was observed, as illustrated in Figure 1b. This corresponds to the heavy fragment resulting from H atom elimination. The photofragment translational energy distribution is shown in Figure 5. It shows that the average translational energy is large, and the peak of the distribution is located at 18 kcal/mol. The electronic potential energy curves along the O−H bond distance are illustrated in Figure 6. A similar repulsive potential along the O−H bond distance was found. The experimental data and potential energy surface calculation suggest that H atom elimination occurs through the following reaction (eq 2):

$$C_2H_5C_6H_4OH \rightarrow C_2H_5C_6H_4O + H \qquad (2)$$

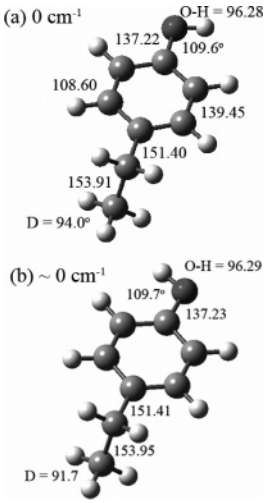

Figure 7. B3LYP/6-311G++(d, p) optimized equilibrium structures and relative energies of the ground-state *p*-ethylphenol of two conformers with selected bond lengths (in pm) and bending angles. D is the dihedral angle between the ethyl backbone and the benzene ring (nearly perpendicular).

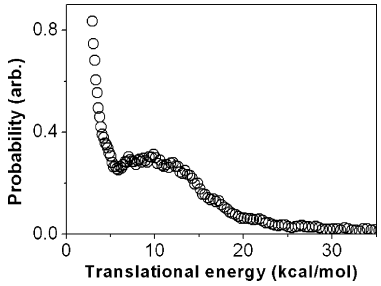

Figure 8. Photofragment translational energy distribution of the reaction $NH_2C_2H_4C_6H_4OH \rightarrow NH_2CH_2 + CH_2C_6H_4OH$.

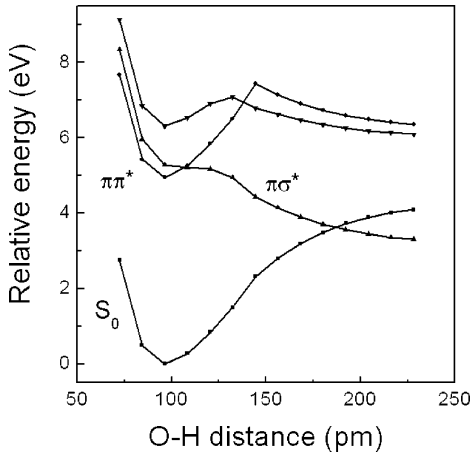

Figure 9. Potential energy curves of *p*-(2-aminoethyl)phenol as functions of the O−H distance calculated at the CASSCF(10,10)/6-311++G(d, p) level.

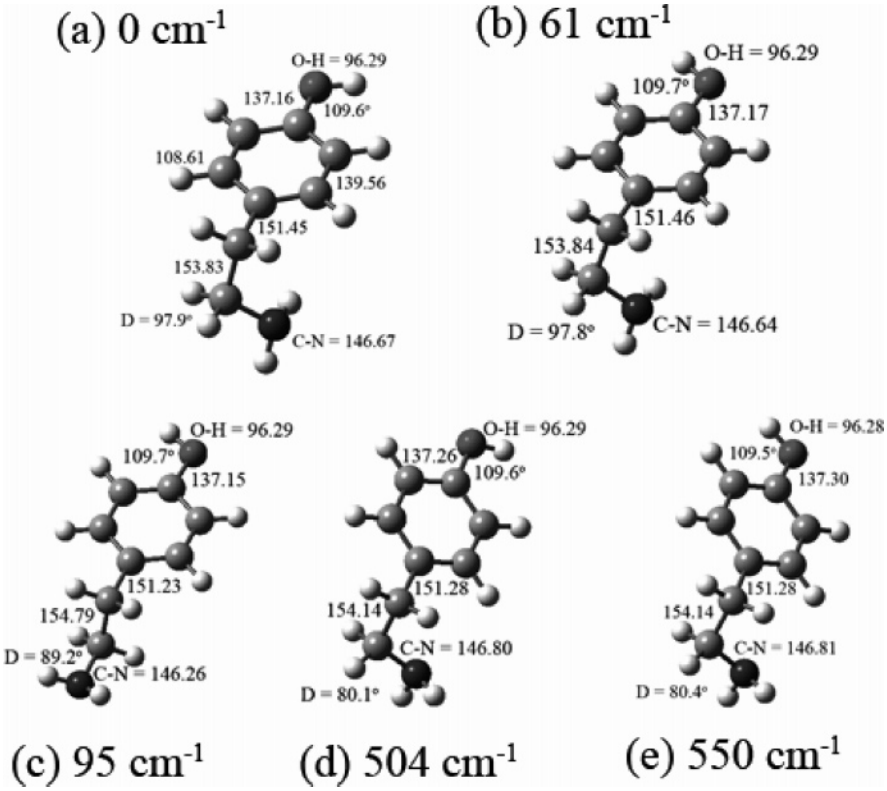

Figure 10. B3LYP/6-311G++(d, p) optimized equilibrium structures and relative energies of the ground-state *p*-(2-aminoethyl)phenol of several conformers with selected bond lengths (in pm) and bending angles. D is the dihedral angle between the ethyl backbone and the benzene ring (nearly perpendicular).

The potential energy curves in Figure 6 were calculated at the ground-state geometry for the most stable conformer. The corresponding structure is shown in Figure 7a. The ground-state structure of the other stable conformer is shown in Figure 7b. From the calculation of the three lowest states at the equilibrium structure of the ground state and in the vicinity of 200 pm, we confirmed the existence of a repulsive potential, $\pi\sigma^*$, along the O−H coordinate for the other conformer.

***p*-(2-Aminoethyl)phenol.** Significantly different photodissociation properties were found from the photodissociation of *p*-(2-aminoethyl)phenol. No fragments corresponding to H atom elimination were observed. Only the fragment ions $m/e = 30$, 106, and 107 were found at 248 nm using the 118 nm photoionization laser beam. Fragment ions $m/e = 106$ and 107 have similar intensity distributions along the velocity axis. It suggests fragment ion $m/e = 106$ results from fragment cracking of $m/e = 107$ due to the excess VUV photon energy. This can be confirmed from the fact that only fragment ions $m/e = 107$ and 30 were observed as the VUV wavelength was changed from 118 to 157 nm. The dissociation can be described by the following reaction (eq 3):

$$NH_2C_2H_4C_6H_4OH \rightarrow NH_2CH_2 + CH_2C_6H_4OH \qquad (3)$$

The photofragment translational energy distribution of the reaction shown in eq 3 is illustrated in Figure 8. It is obvious that there are two components in the distribution. The two components in the distribution indicate that there are at least two mechanisms involved in the dissociation of *p*-(2-aminoethyl)phenol at 248 nm. For the slow component, the average translational energy release is small and the fragment translational energy distribution decreases monotonically with the translational energy. These are typical characteristics of a dissociation from hot molecules. On the other hand, the average released translational energy for the fast component is large, and the peak of the distribution is located far away from zero. These are the characteristics of dissociation from an excited state with a repulsive potential energy surface, or from an electronic state with a large exit barrier height.

Similar translational energy distributions have also been found in the photodissociation of ethylbenzene, propylbenzene, and ethyltoluene at 248 nm.[16−18] For ethylbenzene, propylbenzene, and ethyltoluene, the alkyl group C−C bond cleavage is the major dissociation channel. The photofragment translational energy distributions of these molecules show a slow component and a fast component. Since the alkyl group is not an electronic chromophore at 248 nm, an electronic excited state with a repulsive potential along the C−C bond is not expected to play a role in this photon energy region. The dissociation mechanism was interpreted as the slow component in the translational energy distribution resulting from the ground-state dissociation and the fast component resulting from the triplet-state dissociation. The fast component resulting from the triplet state was confirmed from the ab initio calculation that a large barrier does exist in the exit channel. An analogous dissociation mechanism can also be applied here to explain the photodissociation of *p*-(2-aminoethyl)phenol at 248 nm.

We also performed similar calculations for *p*-(2-aminoethyl)-phenol. Figure 9 shows the electronic potential energy curves along the O−H bond distance of the most stable conformer of *p*-(2-aminoethyl)phenol. The repulsive characteristic of the potential energy surface along the O−H bond distance of *p*-(2-aminoethyl)phenol was observed. The structures of the most stable conformer and the other conformers are illustrated in Figure 10. For the other conformers, we calculated the three lowest electronic states at the equilibrium structure of the ground state and in the vicinity of 200 pm. We confirmed the existence

of a repulsive potential, $\pi\sigma^*$, along the O−H coordinate for all the other conformers.

V. Discussion

The results of these three amino acid chromophores reveal interesting side-chain size-dependent dissociation properties. Since the alkyl group and amino group are not the absorption chromophores at 248 nm, photoexcitation of *p*-methylphenol, *p*-ethylphenol, and *p*-(2-aminoethyl)phenol at 248 nm photons all correspond to the excitation of the phenyl ring. However, the decay of the excited phenyl ring is very different between these three molecules. For both *p*-methylphenol and *p*-ethylphenol, the major relaxation of the excited phenyl ring is through the coupling between the $\pi\pi^*$ and $\pi\sigma^*$ states. As a result, H atom elimination from a repulsive state is the major dissociation channel. These observations demonstrate that the dissociation from the repulsive excited state plays an important role in small tyrosine chromophores, including phenol, *p*-methylphenol, and *p*-ethylphenol. As the side chain changes from H, CH_3, or C_2H_5 to $C_2H_4NH_2$, the dissociation properties change dramatically. The change could be due to two effects from the side chain. First, the change of the location of the repulsive potential energy surface could render it inaccessible under current photoexcitation conditions. However, our calculations show that the repulsive characteristic of the potential energy surface along the O−H bond distance exists in all three molecules. In addition, the energy of the repulsive potential energy surface remains in the same region that the energy from the absorption of 248 nm photon is enough to reach the repulsive part of the potential energy surface, although it does not necessarily indicate that the absorption spectra and coupling strength between the $\pi\pi^*$ and $\pi\sigma^*$ states remains the same. An explanation of the similar electronic potentials of these chromophores is that these states correspond to the transitions from the π orbitals of the benzene ring to the σ^*(OH) and π^* orbitals, while the methyl, ethyl, and aminoethyl groups do not significantly change the electronic structures of these low-lying states.

The other effect of the side-chain is the increase in the S_1-S_0 internal conversion rate and/or S_1-T_1 intersystem crossing rate which competes with the predissociation from the repulsive potential energy surface. Since the internal conversion and intersystem crossing rates are proportional to the density of states, the replacement of a H atom by a side chain increases the density of states substantially due to the low vibrational frequency modes, like torsion, in the side chain. Obviously, the increase of the internal conversion/intersystem crossing rate is not large enough in *p*-methylphenol and *p*-ethylphenol to compete with the predissociation from the repulsive potential energy surface. However, the internal conversion rate or intersystem crossing rate in *p*-(2-aminoethyl)phenol is large enough that the predissociation from the repulsive state is quenched completely.

Internal conversion to the ground state also can occur through the other channel, that is, from the $\pi\sigma^*$ state to the ground state through the second conical intersection in the vicinity of 200 pm. In addition, intersystem crossing can occur via a similar mechanism if a conical intersection between the triple state and the S_2 state exists. Nevertheless, the results of these alternatives in *p*-(2-aminoethyl)phenol are the same, that is, they quench the population of the S_2 state and make the H atom elimination from the repulsive state impossible.

Since the energies of different conformers are very close, more than one conformer existed in the molecular beam. In addition, the rotational barriers for the methyl, ethyl, and 2-aminoethyl groups are about 10−20 cm^{-1} for these molecules calculated at the B3LYP/6-311++G(d, p) level, indicating that they can rotate freely. The results therefore are the averages according to the populations of each conformer in the molecular beam. Although we cannot determine the relative contributions of these conformers, the experimental results show that all of the conformers of methylphenol and ethylphenol existing in the molecular beam only dissociate along the O−H bond on the repulsive potential energy surface. On the other hand, none of the conformers of *p*-(2-aminoethyl)phenol that existed in the molecular beam dissociate on the repulsive potential energy surface. They only dissociate through C−C bond cleavage on the ground state and/or the triplet state.

Comparison of these three chromophores reveals an interesting side-chain effect on the dissociation dynamics. A future challenge is to find out the dissociation dynamics of the conformers that currently do not exist in the molecular beam, the larger chromophores, or tyrosine itself.

Acknowledgment. The work was supported by the National Science Council, Taiwan, under contract number NSC 94-2113-M-001-036, NSC 95-2113-M-142-001-MY2. We are grateful to the National Center for High-Performance Computing for computer time.

References and Notes

(1) Robin, M. B. *Higher Excited States of Polyatomic Molecules*; Academic: New York, 1972.
(2) Crespo-Hernandez, C.; Cohen, E. B.; Hare, P. M.; Kohler, B. *Chem. Rev.* **2004**, *104*, 1977.
(3) Callis, R. *Annu. Rev. Phys. Chem.* **1983**, *34*, 329.
(4) Creed, D. *Photochem. Photobiol.* **1984**, *39*, 537.
(5) Reuther, A.; Iglev, H.; Laenen, R.; Laubereau, A. *Chem. Phys. Lett.* **2000**, *325*, 360.
(6) Sobolewski, A. L.; Domcke, W.; Dedonder-Lardeuxc, C.; Jouvet, C. *Phys. Chem. Chem. Phys.* **2002**, *4*, 1093.
(7) Lan, Z.; Domcke, W.; Vallet, V.; Sobolewski, A. L.; Mahapatra, S. *J. Chem. Phys.* **2005**, *122*, 224315.
(8) Sobolewski, A. L.; Domcke, W. *J. Phys. Chem. A* **2001**, *105*, 9275.
(9) Tseng, C. M.; Lee, Y. T.; Ni, C. K. *J. Chem. Phys.* **2004**, *121*, 2459.
(10) Lin, M. F.; Tseng, C. M.; Lee, Y. T.; Ni, C. K. *J. Chem. Phys.* **2005**, *123*, 124303.
(11) Tsai, S. T.; Lin, C. K.; Lee, Y. T.; Ni, C. K. *J. Chem. Phys.* **2000**, *113*, 67.
(12) Tsai, S. T.; Lin, C. K.; Lee, Y. T.; Ni, C. K. *Rev. Sci. Instrum.* **2001**, *72*, 1963.
(13) Lin, C. K.; Huang, C. L.; Jiang, J. C.; Chang, H.; Lin, S. H.; Lee, Y. T.; Ni, C. K. *J. Am. Chem. Soc.* **2002**, *124*, 4068.
(14) Tseng, C. M.; Dyakov, Y. A.; Huang, C. L.; Mebel, A. M.; Lin, S. H.; Lee, Y. T.; Ni, C. K. *J. Am. Chem. Soc.* **2004**, *126*, 8760.
(15) Werner, H.-J.; Knowles, P. J.; Lindh, R.; Manby, F. R.; Schütz, M.; others, see http://www.molpro.net. *MOLPRO*, version 2006.1, a package of ab initio programs.
(16) Huang, C. L.; Jiang, J. C.; Lin, S. H.; Lee, Y. T.; Ni, C. K. *J. Chem. Phys.* **2002**, *116*, 7779.
(17) Huang, C. L.; Jiang, J. C.; Lin, S. H.; Lee, Y. T.; Ni, C. K. *J. Chem. Phys.* **2002**, *117*, 7034.
(18) Huang, C. L.; Dyakov, Y. A.; Lin, S. H.; Lee, Y. T.; Ni, C. K. *J. Phys. Chem. A* **2005**, *109*, 4995.